Report

Cell Reports

PP1-Mediated Dephosphorylation of Lgl Controls Apical-basal Polarity

Graphical Abstract

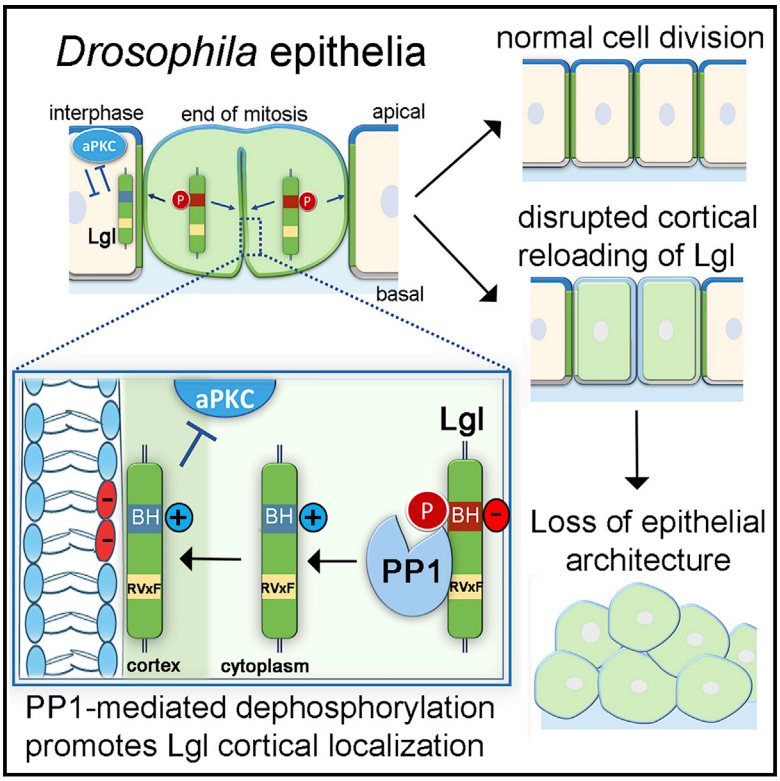

Highlights

- Cytoplasmic Lgl returns to the cortex at mitotic exit in *Drosophila* epithelia
- Lgl cortical localization depends on PP1-mediated dephosphorylation
- PP1 dephosphorylates Lgl to maintain epithelial architecture
- Apical polarization of new daughter cells is coupled with Lgl cortical reloading

Authors

Sofia Moreira, Mariana Osswald, Guilherme Ventura, Margarida Gonçalves, Claudio E. Sunkel, Eurico Morais-de-Sá

Correspondence

eurico.sa@ibmc.up.pt

In Brief

Moreira et al. investigate the post-mitotic polarization of new daughter cells in *Drosophila* epithelia. They identify PP1 phosphatase as a regulator of the conserved basolateral determinant Lgl. Dephosphorylation of Lgl counteracts aPKC/AurA activity, being an essential mechanism to restore Lgl cortical localization and to maintain the architecture of proliferative tissue.

Moreira et al., 2019, Cell Reports *26*, 293–301
January 8, 2019
https://doi.org/10.1016/j.celrep.2018.12.060

CellPress

Cell Reports
Report

PP1-Mediated Dephosphorylation of Lgl Controls Apical-basal Polarity

Sofia Moreira,[1,2] Mariana Osswald,[1,2,3] Guilherme Ventura,[1,2,3,4] Margarida Gonçalves,[1,2] Claudio E. Sunkel,[1,2] and Eurico Morais-de-Sá[1,2,5,*]

[1]Instituto de Biologia Molecular e Celular, Universidade do Porto, Porto, Portugal
[2]Instituto de Investigação e Inovação em Saúde (i3S), Universidade do Porto, Porto, Portugal
[3]These authors contributed equally
[4]Present address: Novo Nordisk Center for Stem Cell Biology (DanStem), University of Copenhagen, Copenhagen, Denmark
[5]Lead Contact
*Correspondence: eurico.sa@ibmc.up.pt
https://doi.org/10.1016/j.celrep.2018.12.060

SUMMARY

Apical-basal polarity is a common trait that underlies epithelial function. Although the asymmetric distribution of cortical polarity proteins works in a functioning equilibrium, it also retains plasticity to accommodate cell division, during which the basolateral determinant Lgl is released from the cortex. Here, we investigated how Lgl restores its cortical localization to maintain the integrity of dividing epithelia. We show that cytoplasmic Lgl is reloaded to the cortex at mitotic exit in *Drosophila* epithelia. Lgl cortical localization depends on protein phosphatase 1, which dephosphorylates Lgl on the serines phosphorylated by aPKC and Aurora A kinases through a mechanism that relies on the regulatory subunit Sds22 and a PP1-interacting RVxF motif of Lgl. This mechanism maintains epithelial polarity and is of particular importance at mitotic exit to couple Lgl cortical reloading with the polarization of the apical domain. Hence, PP1-mediated dephosphorylation of Lgl preserves the apical-basal organization of proliferative epithelia.

INTRODUCTION

Epithelial tissues compartmentalize multicellular organisms and have a variety of specialized roles that rely on asymmetries in protein and lipid composition and the precise positioning of intercellular junctions along its apical-basal axis (Rodriguez-Boulan and Macara, 2014). This polarity axis is defined by conserved apical-basal polarity proteins, which segregate into distinct domains along the epithelial cell cortex (Flores-Benitez and Knust, 2016). One such protein is Lethal giant larvae (Lgl), originally identified as a tumor suppressor in *Drosophila* and often misregulated in human cancer (Gateff, 1978; Halaoui and McCaffrey, 2015). In epithelia, Lgl cooperates with Discs Large (Dlg) and Scribbled as a basolateral determinant to restrict the localization and activity of the atypical protein kinase C (aPKC) and Crumbs complexes to the apical domain (Bilder et al., 2000, 2003; Tanentzapf and Tepass, 2003), possibly by inhibiting aPKC activity (Atwood and Prehoda, 2009; Wirtz-Peitz et al., 2008; Yamanaka et al., 2006) or regulating the trafficking of apical transmembrane proteins (Fletcher et al., 2012; Jossin et al., 2017).

Lgl associates with the actomyosin cytoskeleton (Betschinger et al., 2003; Dahan et al., 2012; Strand et al., 1994), and recent work revealed that its cortical localization is, however, primarily mediated by binding to plasma membrane phosphoinositides through a positively charged basic and hydrophobic (BH) motif (Bailey and Prehoda, 2015; Dong et al., 2015). This motif is phosphorylated by aPKC (Betschinger et al., 2003; Plant et al., 2003) to exclude Lgl from the apical cortex during interphase and by mitotic kinase Aurora A (AurA) to completely release Lgl from the cortex and promote proper mitotic spindle orientation in epithelial tissue (Bell et al., 2015; Carvalho et al., 2015). Interestingly, apical polarity proteins such as aPKC, Par-6, and Par-3 also adjust localization during epithelial mitosis, as shown in *Drosophila* and during early embryogenesis of *Nematostella vectensis* (Bergstralh et al., 2013; Carvalho et al., 2015; Morais-de-Sá and Sunkel, 2013; Ragkousi et al., 2017; Rosa et al., 2015). However, it is unknown how Lgl cortical localization is restored at the end of cell division and how this is coordinated with daughter cell polarization. Moreover, although phosphorylation controls Lgl localization and function, how (and whether) counteracting protein phosphatases actively dephosphorylate Lgl remains undetermined.

Here we report the PP1-Sds22 complex as a critical regulator of Lgl dephosphorylation, promoting its localization at the cortex and plasma membrane. Because dividing cells must deal with the complete pool of Lgl in the cytoplasmic and hyperphosphorylated form, this mechanism has foremost significance to timely polarize daughter cells and maintain the architecture of proliferating epithelia.

RESULTS

Cytoplasmic Lgl Returns to the Cortex at Mitotic Exit

To investigate how Lgl localization is restored in the daughter cells, we examined the dynamics of Lgl subcellular redistribution in the follicular epithelium, a monolayered tissue that envelops the germline in the *Drosophila* ovary. Lgl cytoplasmic levels decline from around 2 min until about 15 min after anaphase onset, with the concomitant accumulation of Lgl at the daughter-daughter (d-d) cell interface just as the new membrane ingresses from the basal side (Figures 1A and 1B; Video S1). This

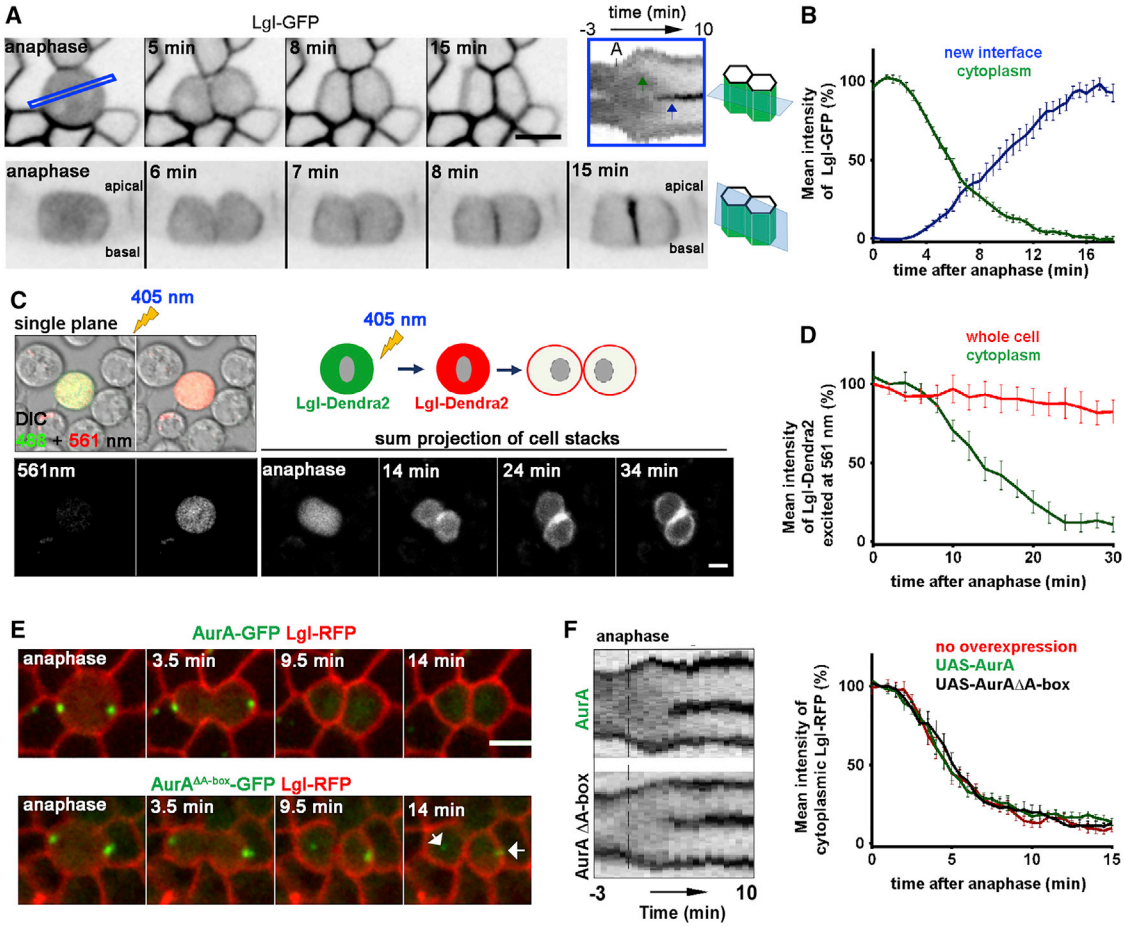

Figure 1. Cytoplasmic Lgl Returns to the Cortex at Mitotic Exit

(A) Dynamic reallocation of Lgl-GFP to the lateral cortex of follicle cells at mitotic exit. A kymograph of the highlighted region shows cytoplasmic decay (green arrow) and Lgl accumulation at the daughter-daughter (d-d) interface (blue arrow).

(B) Normalized mean intensity of Lgl-GFP in the cytoplasm (n = 21) and at the daughter-daughter interface (n = 16) since anaphase.

(C) Photoconversion of Lgl-Dendra2 in mitotic S2 cells shows that cytoplasmic Lgl returns to the cortex at mitotic exit.

(D) Normalized mean intensity of photoconverted Lgl-Dendra2 in the cytoplasm (green) and the integrated density of photoconverted Lgl in the whole cell (red) (n = 6).

(E) Dividing follicle cells expressing Lgl-red fluorescent protein (RFP) and AurA-GFP or AurA$^{\Delta Abox}$-GFP, which is detectable longer at centrosomes (arrows).

(F) Normalized mean intensity of cytoplasmic Lgl-RFP in control cells (red, n = 14) and cells overexpressing AurA-GFP (n = 13) and AurA$^{\Delta Abox}$-GFP (n = 9). The kymographs show the patterns of Lgl-RFP localization.

Data are presented as mean ± SEM. Scale bars, 5 μm.

See also Figure S1.

dynamic reallocation of Lgl-GFP at mitotic exit is also reproduced in the *Drosophila* embryonic epithelium (Figure S1A). To test whether Lgl returns from the cytoplasm to the cortex, we labeled cytoplasmic Lgl through photoconversion during mitosis in S2 cells (Figure 1C). Photoconverted Lgl-Dendra2 accumulates at the cortex when cells exit mitosis (Figure 1C). Moreover, the labeled pool of Lgl-Dendra2 is not degraded during mitotic exit because the total fluorescence of the photoconverted protein remains constant during the period of cytoplasmic signal decay (Figure 1D). Thus, at mitotic exit, Lgl is fully reloaded from the cytoplasm to the cortex. The kinetics of cytoplasmic decay are therefore an accurate readout for the sum of Lgl cortical reloading to the pre-existing cell membranes and to the newly formed daughter-daughter interface.

Lgl release from the cortex at mitotic entry is controlled by AurA (Bell et al., 2015; Carvalho et al., 2015), which is targeted for degradation by the Cdh1-activated anaphase-promoting complex (APC-Cdh1) at mitotic exit (Castro et al., 2002). To investigate whether AurA degradation determines Lgl cortical reloading, we overexpressed AurA-GFP and a stabilized version, AurA$^{\Delta Abox}$-GFP, which lacks the A-box domain and impairs recognition by the APC-Cdh1 complex without interfering with the catalytic domain (Meghini et al., 2016). Stabilization of AurA does not change Lgl dynamics at mitotic exit (Figures 1E and 1F). Moreover, although RNAi depletion of AurA interferes with cortical release at mitotic entry in S2 cells (Carvalho et al., 2015), it does not affect Lgl cortical reloading (Figure S1B). Altogether, we conclude that

regulation of AurA stability is not the timer controlling Lgl reloading to the cortex.

PP1 Antagonizes aPKC and AurA-Mediated Phosphorylation of Lgl

Lgl phosphorylation reduces its affinity to the plasma membrane and to the underlying cortex (Bailey and Prehoda, 2015; Dong et al., 2015; Betschinger et al., 2003). Thus, Lgl cortical reloading should require dephosphorylation, but a phosphatase for Lgl has yet to be described. Two good candidates are PP1 and PP2A, serine and threonine-specific phosphatases activated at mitotic exit (Barr et al., 2011). These phosphatases form multimeric holoenzyme complexes containing catalytic and regulatory subunits. There are four *Drosophila* genes encoding PP1 catalytic subunits: *Pp1β9C* (*flw*), *Pp1-87B*, *Pp1α-96A*, and *Pp1α13C*, which is responsible for negligible PP1 activity, whereas the PP2A catalytic subunit is encoded by *microtubule star* (*mts*). RNAi-mediated depletion of PP1α-96A, Flw, or Mts in the follicular epithelium does not significantly affect Lgl localization (Figures S2A–S2D), whereas PP1-87B depletion leads to Lgl mislocalization to the cytoplasm, as observed by clonal (Figure 2A) and global depletion (Figure 2C).

To confirm whether PP1-87B is the only essential PP1 catalytic subunit required for proper Lgl localization, we generated mutant clones using null alleles of *flw* and *Pp1α-96A*. Lgl localization in these mutant clones is indistinguishable from wild-type cells, whereas Lgl is fully cytoplasmic in double *pp1-87B*, *pp1α-96A* mutant clones (Figure 2B), indicating that PP1-87B enables cortical Lgl localization. This is unlikely to stem from a specific function of PP1-87B but, rather, from it being the most abundant PP1c isozyme because PP1 catalytic subunits have highly overlapping roles (Kirchner et al., 2007). Consistent with this, Lgl cortical localization in PP1-87B-depleted follicle cells is rescued by overexpression of human PPP1cc, whose closest ortholog is *Pp1α-96A* (Figure 2C). Moreover, overexpression of a global PP1 inhibitor, NiPp1, also disrupts Lgl localization (Figure 2D). Thus, overall PP1 activity is essential for proper Lgl localization to the lateral cortex in *Drosophila* epithelia, which is consistent with a role in Lgl dephosphorylation.

We used recombinant MBP-Lgl and Lgl-GFP immunoprecipitated from ovaries to examine whether PP1 could directly dephosphorylate Lgl on S656, an aPKC and AurA phosphorylation site. Incubation of recombinant PP1 with Lgl previously phosphorylated by AurA results in a concentration- and time-dependent decrease in S656 phosphorylation, indicating that Lgl is a substrate for PP1 (Figures 2E and 2F). Importantly, the activity of PP1 toward Lgl is specific compared with λ phosphatase, which fails to dephosphorylate Lgl as efficiently (Figure S2E). Furthermore, we used *Drosophila* S2 cells to dissect whether Lgl mislocalization upon PP1 inactivation results from hyperphosphorylation on the aPKC and AurA phosphorylation sites. Cytoplasmic localization of Lgl is reproduced upon PP1-87B depletion in S2 cells, whereas co-depletion of aPKC rescues Lgl cortical localization (Figures 2G, S2F, and S2G). Moreover, we simultaneously analyzed the localization of Lgl and Lgl^{3A}, which harbors mutations in the serines controlled by aPKC (S656, S660, and S664) and AurA (S656 and S664) (Bell et al., 2015; Betschinger et al., 2003; Carvalho et al., 2015). Strikingly, Lgl^{3A} is retained at the cortex, in contrast with the cytoplasmic accumulation of Lgl in the follicular epithelium and in S2 cells depleted of PP1-87B (Figure 2H). Hence, these results collectively suggest that PP1-mediated dephosphorylation of the aPKC and AurA phosphorylation sites promotes Lgl localization at the lateral cortex.

PP1-Mediated Dephosphorylation of Lgl Maintains Epithelial Architecture and Polarity

PP1-87B RNAi leads to loss of epithelial polarity in the follicular epithelium, with consequent cell invasion and multilayering (Figure S3). This mimics Lgl loss of function phenotypes in the follicular epithelium (Bilder et al., 2000), but PP1 is involved in multiple pathways, which may indirectly contribute to the phenotype. Given that cortical Lgl antagonizes apical determinants, we tested whether reducing aPKC levels could attenuate this phenotype. *aPKC* heterozygosity strongly suppresses the multilayering phenotype of PP1-87B-depleted tissue (Figure 3A), suggesting that PP1 activity balances apical activity by promoting Lgl cortical localization.

Association of PP1 with regulatory subunits and substrates is often mediated by a RVxF docking motif, [KR] $[X]_{0-1}$[VI]{P} [FW], which binds a PP1 hydrophobic pocket (Wakula et al., 2003). Interestingly, Lgl has a sequence that fits this motif and that is widely conserved in metazoans (Figure 3B). To define the functional significance of Lgl dephosphorylation by PP1, we mutated two critical residues of the PP1 docking motif (Meiselbach et al., 2006). In comparison to Lgl-GFP, $Lgl^{K327A,F331A}$-GFP accumulates strongly in the cytoplasm of follicle cells and shows increased S656 phosphorylation (Figures 3C and 3D). More importantly, expression of $Lgl^{K327A,F331A}$-GFP does not support epithelial apical-basal polarity in *lgl*-null mutant clones, leading to multilayered tissue where aPKC is mislocalized (Figures 3E and 3F). Thus, PP1-mediated dephosphorylation promotes Lgl localization to the cortex, where it can act as basolateral determinant to control epithelial organization.

PP1 Orchestrates Apical-basal Polarization at Mitotic Exit

Lgl must be relocated to the epithelial cortex of daughter cells at mitotic exit, making this period particularly challenging for PP1-mediated dephosphorylation of Lgl. Accordingly, Lgl cortical reloading is minor in PP1-87B depleted follicle cells (~70% of mitotic levels remain cytoplasmic 35 min after anaphase onset versus ~20% in the control; Figures 4A and 4B), even for cells that present Lgl largely cortical before mitotic entry (Video S2). Moreover, depletion of the PP1 regulatory subunit Sds22, which enhances PP1 activity during cytokinesis (Kunda et al., 2012; Ohkura and Yanagida, 1991), also delays Lgl reloading at mitotic exit (Figure 4B). Sds22 RNAi has, however, a milder effect than PP1-87B RNAi, culminating in lower levels of cytoplasmic Lgl during early interphase (~40% of mitotic levels). We obtained similar results in *Drosophila* S2 cells (Figure S4A), suggesting that Sds22 is particularly significant to boost PP1 activity to deal with the complete pool of phosphorylated and cytoplasmic Lgl at mitotic exit. $Lgl^{K327A,F331A}$ also shows disrupted cytoplasmic decay in both the embryonic and

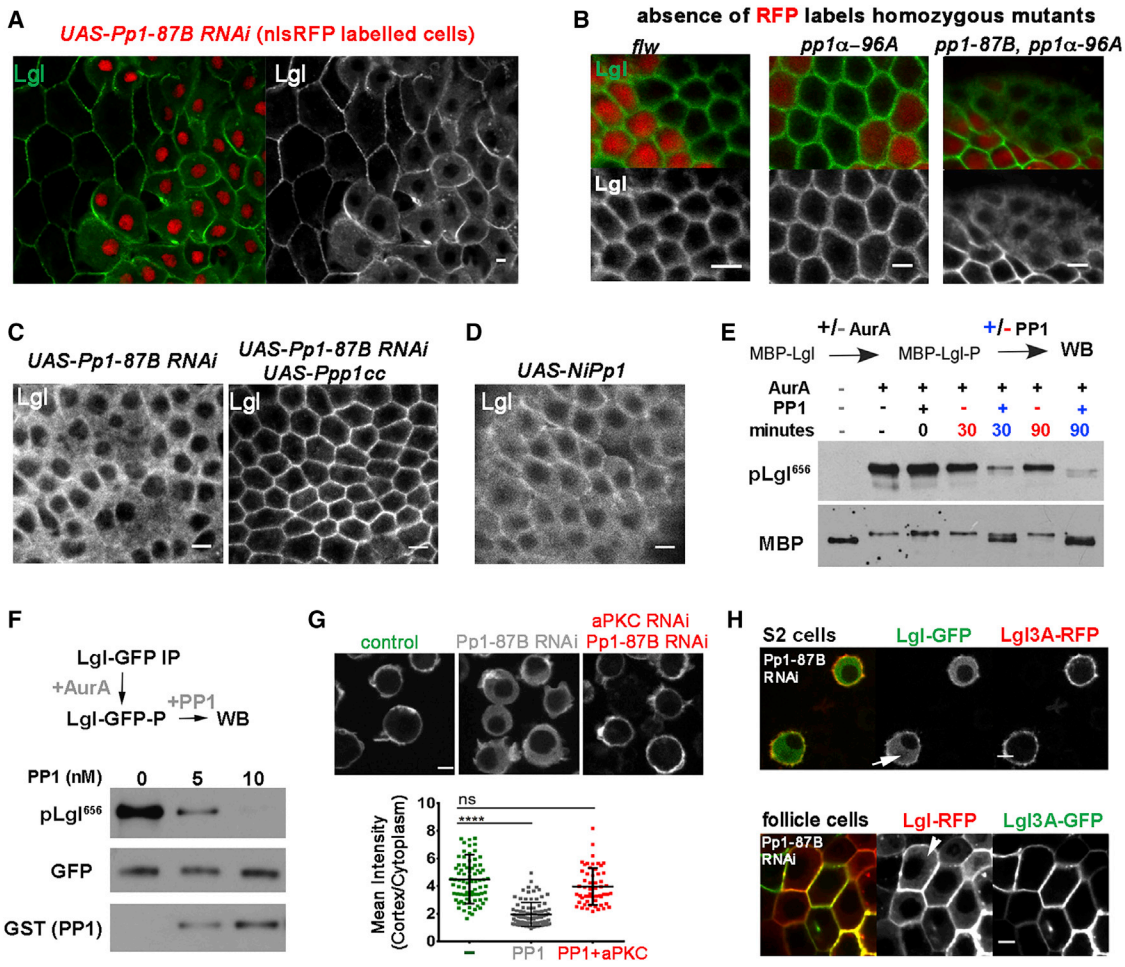

Figure 2. PP1 Antagonizes aPKC/AurA Phosphorylation to Control Lgl Cortical Localization

(A and B) Follicular epithelium stained with anti-Lgl (A) upon clonal depletion of PP1-87B by RNAi (labeled with nuclear localization signal-red fluorescent protein [nlsRFP]) and in (B) egg chambers with mutant clones (absence of nlsRFP) for flw^{FP41}, $pp1\alpha\text{-}96A^{2}$, or $pp1\text{-}87B^{87Bg\text{-}3}$, $pp1\alpha\text{-}96A^{2}$.

(C) Disruption of Lgl localization by PP1-87B RNAi (100%, n = 40) is rescued by overexpression of the human PPP1CC (normal localization, 88%; n = 34).

(D) Overexpression of the PP1 inhibitor NiPp1 induces Lgl-GFP cytoplasmic localization.

(E and F) Western blot analysis of an *in vitro* dephosphorylation assay performed after Lgl phosphorylation by AurA. Dephosphorylation by GST-PP1γ of (E) recombinant maltose binding protein (MBP)-Lgl and (F) Lgl-GFP immunoprecipitated from ovary extracts was detected using a S656 phosphospecific antibody. Blots were also probed for (E) MBP, (F) GFP, and glutathione S-transferase (GST) as controls.

(G) PP1-87B RNAi in S2 cells induces Lgl cytoplasmic mislocalization, which is rescued by simultaneous aPKC depletion. The cortex/cytoplasmic intensity ratio is plotted. Mean ± SD (n = 79 for control, n = 94 for PP1-87B RNAi and n = 74 for PP1-87B RNAi + aPKC RNAi). The p value was calculated with one-way ANOVA ($p < 0.0001$).

(H) Images of S2 cells and follicle cells depleted for PP1-87B by RNAi and co-expressing fluorescently tagged Lgl and Lgl^{3A}.

Scale bars, 5 μm.

See also Figure S2.

follicular epithelium (Figures 4C, 4D, and S4B). Nevertheless, $Lgl^{K327A,F331A}$-GFP cytoplasmic decay is much faster than Lgl-GFP in PP1-87B-depleted follicle cells. Because Sds22 RNAi induces strong cytoplasmic retention of $Lgl^{K327A,F331A}$-GFP (Figure 4C and 4D), we conclude that this PP1-docking motif promotes robust dephosphorylation but is dispensable for partial PP1 activity when the PP1-Sds22 complex is available.

In many proliferative tissues, a new daughter-daughter interface is formed upon cell division to hold daughter cells together (Firmino et al., 2016; Herszterg et al., 2014; Olivier et al., 2010). We investigated the importance of Lgl cortical reloading for daughter-daughter interface polarization by examining the segregation of its mutual antagonist aPKC to the apical domain. Simultaneous imaging of Lgl-mCherry with aPKC-GFP shows that Lgl starts localizing to the lateral cortex before apical accumulation of aPKC (Figure 4E, kymographs). This likely results from the basal-to-apical ingression of the cytokinetic furrow, described previously in many epithelia (Herszterg et al., 2014; Morais-de-Sá and Sunkel, 2013). Moreover, Lgl accumulation

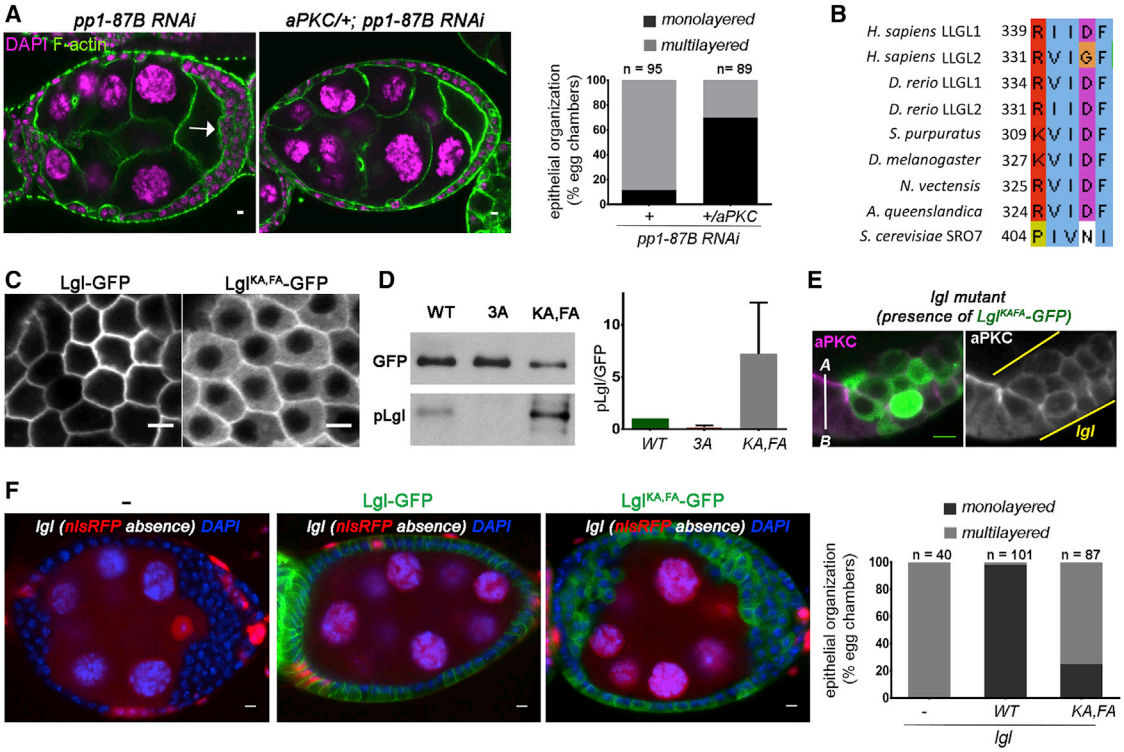

Figure 3. PP1-Mediated Dephosphorylation of Lgl Maintains Epithelial Architecture

(A) Egg chambers stained for F-actin and DAPI. The plot depicts the percentage of egg chambers (stage 4 to stage 8) with multilayered follicular epithelium (arrow) in *tj-Gal4/+;UAS-Pp1-87B RNAi/+* (~88% multilayering) and *tj-Gal4/aPKC^{k06403};UAS-Pp1-87B RNAi/+* (~30% multilayering) flies.

(B) Aligned amino acid sequences of the putative PP1-docking site motif.

(C) Lgl^{K327A,F331A}–GFP shows a stronger accumulation in the follicle cell cytoplasm than Lgl-GFP.

(D) Western blot of protein extracts from ovaries with expression of Lgl-GFP (WT), Lgl^{3A}-GFP (3A), and Lgl^{K327A,F331A}-GFP (KA, FA). Blots were probed with a S656 phosphospecific antibody (pLgl) and anti-GFP. The pLgl/GFP ratio was determined in three independent experiments and normalized to the WT (mean ± SEM is shown).

(E and F) Lgl^{K327A,F331A}-GFP does not sustain epithelial polarity and monolayered organization. Shown are mosaic egg chambers of *lgl^{27S3}* mutant follicle cell clones marked with the expression of Lgl^{K327A,F331A}-GFP (GAL80 absence) and stained for aPKC (E) and *lgl^{27S3}* mutant clones marked by absence of RFP and with general expression of the indicated Lgl variant in the follicular epithelium (F). DAPI staining is also shown. The graph includes data from 3 independent experiments quantifying mutant clones larger than 1/4 of stage 6–stage 8 egg chambers.

Scale bars, 5 μm.

See also Figure S3.

is completed before aPKC reaches maximum apical levels (Figure 4E, kymographs). We therefore hypothesized that loading Lgl to the lateral cortex could be necessary for aPKC accumulation at the apical side. To test this idea, we used an *lgl* temperature-sensitive allele, *lgl^{ts3}*, which reallocates to the cytoplasm at restrictive temperature (Manfruelli et al., 1996), and limited our analysis to the first 2 hr at 29°C, during which the tissue maintains its monolayered organization (Figure S4B). aPKC accumulation in the apical daughter-daughter interface is drastically impaired in *lgl^{ts3}/lgl^{4}* mutant follicle cells (Figure 4F). Moreover, aPKC localizes ectopically in the lateral domain at the daughter-daughter interface of *lgl^{ts3}/lgl^{4}* mutant cells (Figure 4G; Video S3), suggesting that Lgl cortical reloading restricts aPKC to the apical side by limiting its lateral accumulation. Thus, by controlling the timing of Lgl cortical reloading, PP1 activation synchronizes the polarization of apical and basolateral domains at mitotic exit.

DISCUSSION

Apical-basal polarity relies on the asymmetric distribution of the polarity determinant Lgl to the lateral cortex of epithelial cells. Research regarding Lgl regulation has been focused on the modulation of phosphorylation via aPKC and Aurora kinases. Here we found that PP1 provides another layer of regulation, antagonizing Lgl phosphorylation by aPKC or AurA. We show that PP1-mediated dephosphorylation can control Lgl subcellular distribution in both epithelial and non-epithelial cells and is critical to maintain the monolayered organization and apical-basal polarity. Because Lgl is a general cell polarity regulator (Betschinger et al., 2003; Dahan et al., 2012; Raman et al., 2016) and also controls the Notch and Hippo signaling pathways (Grusche et al., 2011; Parsons et al., 2014), it is likely that the significance of Lgl regulation by PP1 extends to a range of processes, including asymmetric cell division, cell migration, fate specification, and growth control.

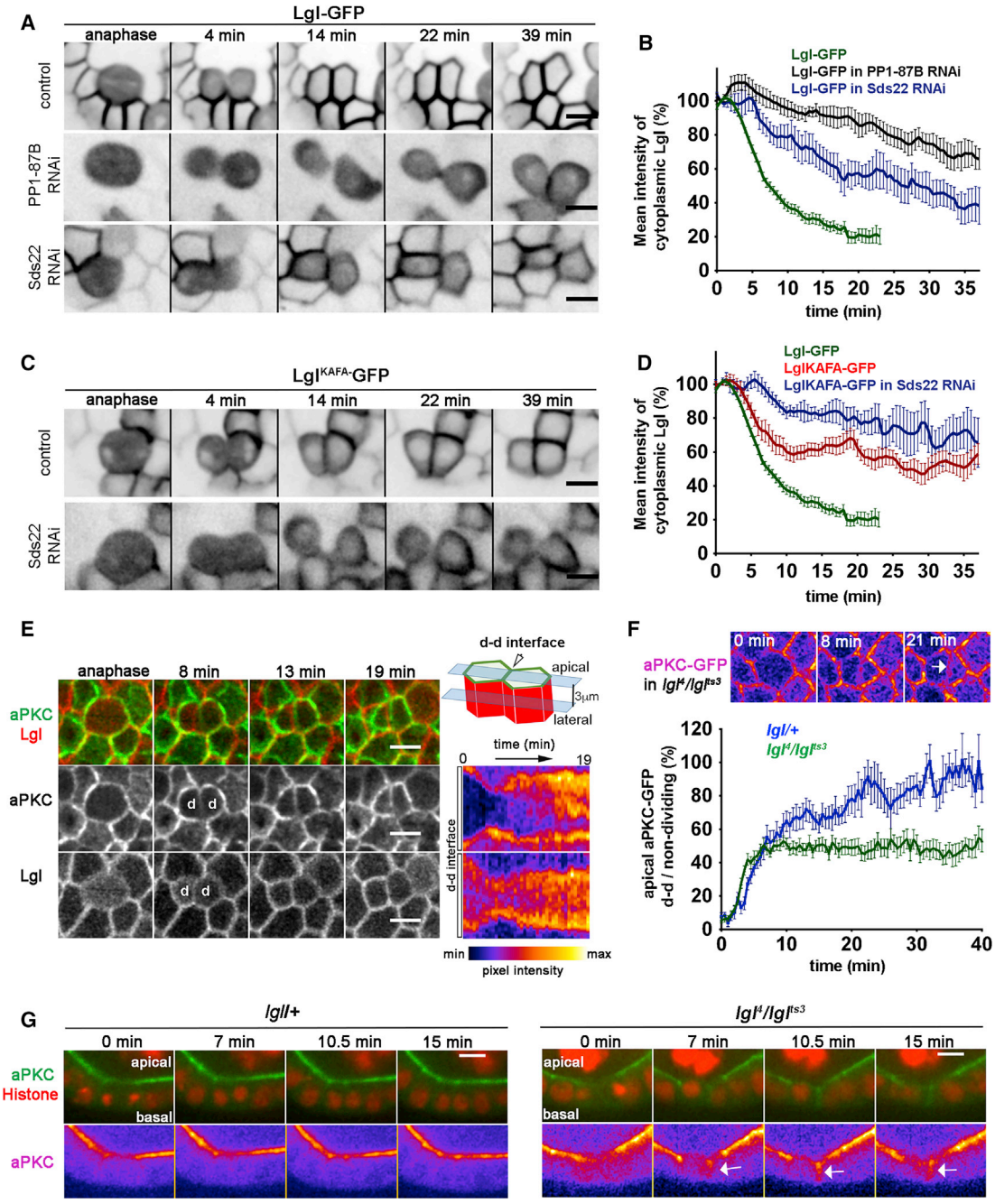

Figure 4. PP1-Mediated Dephosphorylation of Lgl Promotes Apical-basal Polarization at Mitotic Exit

(A) Disrupted cortical reloading of Lgl in PP1-87B- and Sds22-depleted follicle cells.

(B) Normalized mean intensity of cytoplasmic Lgl-GFP in control (n = 22, also in D), PP1-87B RNAi (n = 8), and Sds22 RNAi (n = 11).

(C) Defects in cortical reloading of Lgl^{K327A,F331A}-GFP are enhanced by Sds22 depletion.

(D) Normalized mean intensity of cytoplasmic Lgl^{K327A,F331A}-GFP in control (n = 11) and Sds22 RNAi (n = 12).

(E) Time-lapse images of follicle cells expressing aPKC-GFP and Lgl-mCherry at endogenous levels. The kymographs (pseudocolored to intensity) detail their accumulation at the daughter-daughter interface, projected in the selected apical and lateral planes, respectively.

(F) aPKC-GFP accumulation in the daughter-daughter interface (arrow, fluorescence intensity normalized to non-dividing cells) is strongly reduced in *lgl*^{4}/*lgl*^{ts3} mutant cells imaged at restrictive temperature (n = 40) (~50% of *lgl*/+, n = 21).

(G) Time-lapse images of midsagittal egg chamber sections show that aPKC-GFP accumulates in the lateral side of the new daughter-daughter interface in *lgl*^{4}/*lgl*^{ts3} mutant cells (arrows) imaged at restrictive temperature.

Time is shown since anaphase. Data show mean ± SEM. Scale bars, 5 μm.

See also Figure S4.

PP1 directly dephosphorylates Lgl, and we show that Lgl localization is insensitive to PP1 depletion when the aPKC and AurA phosphorylation sites are mutated. Thus, PP1 dephosphorylation promotes the phosphorylation-inhibited binding between the BH motif of Lgl and plasma membrane phosphoinositides (Bailey and Prehoda, 2015; Dong et al., 2015). This mode of regulation parallels cell polarization in fission yeast, where the protein phosphatase 1 complex Tea4-Dis2 controls dephosphorylation of the polarity regulator Pom1 to expose a basic region with affinity for plasma membrane phospholipids (Hachet et al., 2011). Furthermore, PP1 has been shown to dephosphorylate Par-3 on aPKC phosphorylation sites (Traweger et al., 2008). PP1 is therefore a critical regulator of cell polarity and antagonizes aPKC activity over multiple substrates in epithelial tissues.

We also show that Sds22 promotes Lgl cortical localization. Sds22 has been identified previously as a regulator of epithelial organization, but this function has been mostly linked to the deleterious effect of myosin or moesin hyperphosphorylation (Grusche et al., 2009; Jiang et al., 2011). Interestingly, similarly to loss of function of the basolateral polarity proteins Scrib, Dlg, and Lgl, *sds22* mutation also promotes neoplastic tumor development in *Drosophila* imaginal discs (Jiang et al., 2011). Thus, the role of the PP1-Sds22 complex in Lgl cortical localization provides a possible mechanistic interpretation for the tumor-suppressive role of Sds22 and its human homolog PPP1R7 (Jiang et al., 2011; Narayan et al., 2003).

Lgl becomes fully cytoplasmic because of AurA phosphorylation at mitotic entry (Bell et al., 2015; Carvalho et al., 2015), and since preexisting phosphorylated Lgl is not degraded, PP1-mediated dephosphorylation is critical to reload cytoplasmic Lgl to the cortex of the daughter cells. Moreover, we show that cortically localized Lgl inhibits aPKC accumulation at the lateral domain of the newly formed interface between daughter cells, promoting its apical localization. Hence, although asymmetric furrow ingression and apical midbody positioning may assist with the establishment of apical-basal asymmetries at mitotic exit (Herszterg et al., 2014; Morais-de-Sá and Sunkel, 2013), PP1-mediated cortical reloading of Lgl plays an essential role in the *de novo* polarization of the daughter-daughter interface. PP1 is tightly regulated throughout the cell cycle, being reactivated at mitotic exit to dephosphorylate a number of mitotic proteins (Kunda et al., 2012; Moura et al., 2017; Wu et al., 2009). This study reveals how the cell cycle-dependent control of PP1 activity also plays an essential role in the context of apical-basal polarity, coupling cell division with the post-mitotic polarization of epithelial cells.

STAR★METHODS

Detailed methods are provided in the online version of this paper and include the following:

- KEY RESOURCES TABLE
- CONTACT FOR REAGENT AND RESOURCE SHARING
- EXPERIMENTAL MODEL AND SUBJECT DETAILS
  - *Drosophila* stocks and genetics
  - *Drosophila* cell culture
- METHOD DETAILS
  - S2 cell stable lines and RNA interference
  - Preparation of ovary and S2 cell protein extracts
  - Immunofluorescence and F-actin staining
  - Cloning of Lgl variants
  - RT-PCR
  - Protein purification
  - *in vitro* dephosphorylation assays
  - Photoconversion experiments in S2 cells
  - Multiple sequence alignments
  - Imaging
- QUANTIFICATION AND STATISTICAL ANALYSIS
  - Cytoplasmic decay of Lgl
  - Lgl accumulation in daughter-daughter interface
  - Intensity of Lgl-Dendra2 upon photoconversion
  - aPKC accumulation in the apical interface formed between daughter cells
  - Interphase cortical/cytoplasmic intensity ratio of Lgl in S2 cells

SUPPLEMENTAL INFORMATION

Supplemental Information includes four figures, one table, and three videos and can be found with this article online at https://doi.org/10.1016/j.celrep.2018.12.060.

ACKNOWLEDGMENTS

We thank Daniel St Johnston, François Schweisguth, Guilles Hickson, Jürgen Knoblich, Torcato Martins, Yang Hong, and the Bloomington Drosophila Stock Center for providing plasmids and fly stocks. This work was funded by national funds through Fundação para a Ciência e a Tecnologia (FCT) under project PTDC/BEX-BCM/0432/2014. This work has also received funding from the project Norte-01-0145-FEDER-000029, supported by Norte Portugal Regional Operational Program (NORTE 2020). E.M. holds an FCT Investigator position. S.M. and M.G. are supported by FCT PhD grants. M.O. is supported by a fellowship from FCT and the GABBA PhD program from the University of Porto.

AUTHORS CONTRIBUTIONS

Conceptualization, S.M. and E.M.; Methodology, S.M., M.O., G.V., and E.M.; Formal Analysis, S.M., M.O., G.V., and E.M.; Investigation, S.M., M.O., G.V., M.G., and E.M.; Writing – Original Draft, E.M.; Writing – Review & Editing, S.M., M.O., G.V., C.S., and E.M.; Supervision, C.S. and E.M.; Funding Acquisition, E.M.

DECLARATION OF INTERESTS

The authors declare no competing interests.

Received: August 1, 2018
Revised: November 23, 2018
Accepted: December 13, 2018
Published: January 8, 2019

REFERENCES

Atwood, S.X., and Prehoda, K.E. (2009). aPKC phosphorylates Miranda to polarize fate determinants during neuroblast asymmetric cell division. Curr. Biol. *19*, 723–729.

Bailey, M.J., and Prehoda, K.E. (2015). Establishment of Par-Polarized Cortical Domains via Phosphoregulated Membrane Motifs. Dev. Cell *35*, 199–210.

Barr, F.A., Elliott, P.R., and Gruneberg, U. (2011). Protein phosphatases and the regulation of mitosis. J. Cell Sci. *124*, 2323–2334.

Bell, G.P., Fletcher, G.C., Brain, R., and Thompson, B.J. (2015). Aurora kinases phosphorylate Lgl to induce mitotic spindle orientation in Drosophila epithelia. Curr. Biol. *25*, 61–68.

Berdnik, D., and Knoblich, J.A. (2002). Drosophila Aurora-A is required for centrosome maturation and actin-dependent asymmetric protein localization during mitosis. Curr. Biol. *12*, 640–647.

Bergstralh, D.T., Lovegrove, H.E., and St Johnston, D. (2013). Discs large links spindle orientation to apical-basal polarity in Drosophila epithelia. Curr. Biol. *23*, 1707–1712.

Besson, C., Bernard, F., Corson, F., Rouault, H., Reynaud, E., Keder, A., Mazouni, K., and Schweisguth, F. (2015). Planar Cell Polarity Breaks the Symmetry of PAR Protein Distribution prior to Mitosis in Drosophila Sensory Organ Precursor Cells. Curr. Biol. *25*, 1104–1110.

Betschinger, J., Mechtler, K., and Knoblich, J.A. (2003). The Par complex directs asymmetric cell division by phosphorylating the cytoskeletal protein Lgl. Nature *422*, 326–330.

Bilder, D., Li, M., and Perrimon, N. (2000). Cooperative regulation of cell polarity and growth by Drosophila tumor suppressors. Science *289*, 113–116.

Bilder, D., Schober, M., and Perrimon, N. (2003). Integrated activity of PDZ protein complexes regulates epithelial polarity. Nat. Cell Biol. *5*, 53–58.

Carvalho, C.A., Moreira, S., Ventura, G., Sunkel, C.E., and Morais-de-Sá, E. (2015). Aurora A triggers Lgl cortical release during symmetric division to control planar spindle orientation. Curr. Biol. *25*, 53–60.

Castro, A., Arlot-Bonnemains, Y., Vigneron, S., Labbé, J.C., Prigent, C., and Lorca, T. (2002). APC/Fizzy-Related targets Aurora-A kinase for proteolysis. EMBO Rep. *3*, 457–462.

Dahan, I., Yearim, A., Touboul, Y., and Ravid, S. (2012). The tumor suppressor Lgl1 regulates NMII-A cellular distribution and focal adhesion morphology to optimize cell migration. Mol. Biol. Cell *23*, 591–601.

Dong, W., Zhang, X., Liu, W., Chen, Y.J., Huang, J., Austin, E., Celotto, A.M., Jiang, W.Z., Palladino, M.J., Jiang, Y., et al. (2015). A conserved polybasic domain mediates plasma membrane targeting of Lgl and its regulation by hypoxia. J. Cell Biol. *211*, 273–286.

Firmino, J., Rocancourt, D., Saadaoui, M., Moreau, C., and Gros, J. (2016). Cell Division Drives Epithelial Cell Rearrangements during Gastrulation in Chick. Dev. Cell *36*, 249–261.

Fletcher, G.C., Lucas, E.P., Brain, R., Tournier, A., and Thompson, B.J. (2012). Positive feedback and mutual antagonism combine to polarize Crumbs in the Drosophila follicle cell epithelium. Curr. Biol. *22*, 1116–1122.

Flores-Benitez, D., and Knust, E. (2016). Dynamics of epithelial cell polarity in Drosophila: how to regulate the regulators? Curr. Opin. Cell Biol. *42*, 13–21.

Gateff, E. (1978). Malignant neoplasms of genetic origin in Drosophila melanogaster. Science *200*, 1448–1459.

Grusche, F.A., Hidalgo, C., Fletcher, G., Sung, H.H., Sahai, E., and Thompson, B.J. (2009). Sds22, a PP1 phosphatase regulatory subunit, regulates epithelial cell polarity and shape [Sds22 in epithelial morphology]. BMC Dev. Biol. *9*, 14.

Grusche, F.A., Degoutin, J.L., Richardson, H.E., and Harvey, K.F. (2011). The Salvador/Warts/Hippo pathway controls regenerative tissue growth in Drosophila melanogaster. Dev. Biol. *350*, 255–266.

Hachet, O., Berthelot-Grosjean, M., Kokkoris, K., Vincenzetti, V., Moosbrugger, J., and Martin, S.G. (2011). A phosphorylation cycle shapes gradients of the DYRK family kinase Pom1 at the plasma membrane. Cell *145*, 1116–1128.

Halaoui, R., and McCaffrey, L. (2015). Rewiring cell polarity signaling in cancer. Oncogene *34*, 939–950.

Heller, D., Hoppe, A., Restrepo, S., Gatti, L., Tournier, A.L., Tapon, N., Basler, K., and Mao, Y. (2016). EpiTools: An Open-Source Image Analysis Toolkit for Quantifying Epithelial Growth Dynamics. Dev. Cell *36*, 103–116.

Herszterg, S., Pinheiro, D., and Bellaïche, Y. (2014). A multicellular view of cytokinesis in epithelial tissue. Trends Cell Biol. *24*, 285–293.

Jiang, Y., Scott, K.L., Kwak, S.J., Chen, R., and Mardon, G. (2011). Sds22/PP1 links epithelial integrity and tumor suppression via regulation of myosin II and JNK signaling. Oncogene *30*, 3248–3260.

Jossin, Y., Lee, M., Klezovitch, O., Kon, E., Cossard, A., Lien, W.H., Fernandez, T.E., Cooper, J.A., and Vasioukhin, V. (2017). Llgl1 Connects Cell Polarity with Cell-Cell Adhesion in Embryonic Neural Stem Cells. Dev. Cell *41*, 481–495.e5.

Kirchner, J., Gross, S., Bennett, D., and Alphey, L. (2007). Essential, overlapping and redundant roles of the Drosophila protein phosphatase 1 alpha and 1 beta genes. Genetics *176*, 273–281.

Kunda, P., Rodrigues, N.T., Moeendarbary, E., Liu, T., Ivetic, A., Charras, G., and Baum, B. (2012). PP1-mediated moesin dephosphorylation couples polar relaxation to mitotic exit. Curr. Biol. *22*, 231–236.

Manfruelli, P., Arquier, N., Hanratty, W.P., and Sémériva, M. (1996). The tumor suppressor gene, lethal(2)giant larvae (l(2)g1), is required for cell shape change of epithelial cells during Drosophila development. Development *122*, 2283–2294.

Meghini, F., Martins, T., Tait, X., Fujimitsu, K., Yamano, H., Glover, D.M., and Kimata, Y. (2016). Targeting of Fzr/Cdh1 for timely activation of the APC/C at the centrosome during mitotic exit. Nat. Commun. *7*, 12607.

Meiselbach, H., Sticht, H., and Enz, R. (2006). Structural analysis of the protein phosphatase 1 docking motif: molecular description of binding specificities identifies interacting proteins. Chem. Biol. *13*, 49–59.

Morais-de-Sá, E., and Sunkel, C. (2013). Adherens junctions determine the apical position of the midbody during follicular epithelial cell division. EMBO Rep. *14*, 696–703.

Moura, M., Osswald, M., Leça, N., Barbosa, J., Pereira, A.J., Maiato, H., Sunkel, C.E., and Conde, C. (2017). Protein Phosphatase 1 inactivates Mps1 to ensure efficient Spindle Assembly Checkpoint silencing. eLife *6*, e25366.

Narayan, G., Pulido, H.A., Koul, S., Lu, X.Y., Harris, C.P., Yeh, Y.A., Vargas, H., Posso, H., Terry, M.B., Gissmann, L., et al. (2003). Genetic analysis identifies putative tumor suppressor sites at 2q35-q36.1 and 2q36.3-q37.1 involved in cervical cancer progression. Oncogene *22*, 3489–3499.

Ohkura, H., and Yanagida, M. (1991). S. pombe gene sds22+ essential for a midmitotic transition encodes a leucine-rich repeat protein that positively modulates protein phosphatase-1. Cell *64*, 149–157.

Olivier, N., Luengo-Oroz, M.A., Duloquin, L., Faure, E., Savy, T., Veilleux, I., Solinas, X., Débarre, D., Bourgine, P., Santos, A., et al. (2010). Cell lineage reconstruction of early zebrafish embryos using label-free nonlinear microscopy. Science *329*, 967–971.

Parsons, L.M., Portela, M., Grzeschik, N.A., and Richardson, H.E. (2014). Lgl regulates Notch signaling via endocytosis, independently of the apical aPKC-Par6-Baz polarity complex. Curr. Biol. *24*, 2073–2084.

Plant, P.J., Fawcett, J.P., Lin, D.C., Holdorf, A.D., Binns, K., Kulkarni, S., and Pawson, T. (2003). A polarity complex of mPar-6 and atypical PKC binds, phosphorylates and regulates mammalian Lgl. Nat. Cell Biol. *5*, 301–308.

Ragkousi, K., Marr, K., McKinney, S., Ellington, L., and Gibson, M.C. (2017). Cell-Cycle-Coupled Oscillations in Apical Polarity and Intercellular Contact Maintain Order in Embryonic Epithelia. Curr. Biol. *27*, 1381–1386.

Raman, R., Damle, I., Rote, R., Banerjee, S., Dingare, C., and Sonawane, M. (2016). aPKC regulates apical localization of Lgl to restrict elongation of microridges in developing zebrafish epidermis. Nat. Commun. *7*, 11643.

Rodriguez-Boulan, E., and Macara, I.G. (2014). Organization and execution of the epithelial polarity programme. Nat. Rev. Mol. Cell Biol. *15*, 225–242.

Rosa, A., Vlassaks, E., Pichaud, F., and Baum, B. (2015). Ect2/Pbl acts via Rho and polarity proteins to direct the assembly of an isotropic actomyosin cortex upon mitotic entry. Dev. Cell *32*, 604–616.

Schindelin, J., Arganda-Carreras, I., Frise, E., Kaynig, V., Longair, M., Pietzsch, T., Preibisch, S., Rueden, C., Saalfeld, S., Schmid, B., et al. (2012). Fiji: an open-source platform for biological-image analysis. Nat. Methods *9*, 676–682.

Strand, D., Jakobs, R., Merdes, G., Neumann, B., Kalmes, A., Heid, H.W., Husmann, I., and Mechler, B.M. (1994). The Drosophila lethal(2)giant larvae tumor suppressor protein forms homo-oligomers and is associated with nonmuscle myosin II heavy chain. J. Cell Biol. *127*, 1361–1373.

Tanentzapf, G., and Tepass, U. (2003). Interactions between the crumbs, lethal giant larvae and bazooka pathways in epithelial polarization. Nat. Cell Biol. *5*, 46–52.

Traweger, A., Wiggin, G., Taylor, L., Tate, S.A., Metalnikov, P., and Pawson, T. (2008). Protein phosphatase 1 regulates the phosphorylation state of the polarity scaffold Par-3. Proc. Natl. Acad. Sci. USA *105*, 10402–10407.

Wakula, P., Beullens, M., Ceulemans, H., Stalmans, W., and Bollen, M. (2003). Degeneracy and function of the ubiquitous RVXF motif that mediates binding to protein phosphatase-1. J. Biol. Chem. *278*, 18817–18823.

Wirtz-Peitz, F., Nishimura, T., and Knoblich, J.A. (2008). Linking cell cycle to asymmetric division: Aurora-A phosphorylates the Par complex to regulate Numb localization. Cell *135*, 161–173.

Wu, J.Q., Guo, J.Y., Tang, W., Yang, C.S., Freel, C.D., Chen, C., Nairn, A.C., and Kornbluth, S. (2009). PP1-mediated dephosphorylation of phosphoproteins at mitotic exit is controlled by inhibitor-1 and PP1 phosphorylation. Nat. Cell Biol. *11*, 644–651.

Yamanaka, T., Horikoshi, Y., Izumi, N., Suzuki, A., Mizuno, K., and Ohno, S. (2006). Lgl mediates apical domain disassembly by suppressing the PAR-3-aPKC-PAR-6 complex to orient apical membrane polarity. J. Cell Sci. *119*, 2107–2118.

STAR★METHODS

KEY RESOURCES TABLE

REAGENT or RESOURCE	SOURCE	IDENTIFIER
Antibodies and F-actin staining		
Rabbit anti-Lgl (d-300) (1:100)	Santa Cruz Biotech	Cat#sc-98260; RRID: AB_1564606
Rabbit anti-aPKC (c-20) (1:500)	Santa Cruz Biotech	Cat#sc-216-G; RRID: AB_632241
Rabbit p-Lgl656 (1:500)	Carvalho et al., 2015	N/A
Rabbit anti-GFP (1:1000)	i3S (Biochemical and Biophysical Technologies)	N/A
Anti-MBP-HRP conjugated (1:10000)	New England Biolabs	Cat#E8038; RRID: AB_1559738
Phalloidin-TRITC	SIGMA-ALDRICH	Cat#P1951; RRID: AB_2315148
Mouse anti-GST (B-14) (1:1000)	Santa Cruz Biotech	Cat#sc-138; RRID: AB_627677
Chemicals, Peptides, and Recombinant Proteins		
Phusion High Fidelity DNA polymerase	New England Biolabs	Cat#M0530S
DreamTaq DNA polymerase	Thermo Fisher Scientific	*Cat#EP0701*
DpnI	New England Biolabs	Cat#R0176S
SuperScript II Reverse Transcriptase	Invitrogen (Life technology)	Cat#18064014
Cellfectin II Reagent	Invitrogen (Life technology)	*Cat#10362100*
Effectene Transfection Reagent	QIAGEN	Cat#301425
GFP-Trap_MA system	ChromoTek GmbH	Cat#gtma-10
Aurora A	Millipore	Cat#14-511
GST-PP1γ	MRC-PPU Reagents (University of Dundee)	N/A
Protein Phosphatase 1	New England Biolabs	Cat#P0754
Lambda Phosphatase	New England Biolabs	Cat#P0753S
Aur A inhibitor MLN8237 (Alisertib)	Selleckchem.com	Cat#S1133
VECTASHIELD with DAPI	Vector Laboratories	Cat#H-1200
Halocarbon oil 700	SIGMA-ALDRICH	Cat#H8898
10S VOLTALEF	VWR chemicals	Cat#24627.188
Paraformaldehyde 20%	Electron Microscopy Sciences	Cat#15713
TWEEN 20	SIGMA-ALDRICH	Cat#P9416
Insulin solution from bovine pancreas	SIGMA-ALDRICH	Cat#I0516
Schneider's insect medium	SIGMA-ALDRICH	Cat#S0146
Fetal Bovine Serum (FBS), heat inactivated	Thermo Fisher	Cat#10500-064
Critical Commercial Assays		
Gateway LR Clonase II Enzyme Mix	Invitrogen (Life Technologies)	Cat#11791-020 and 11791-100
RNeasy Mini Kit	QIAGEN	Cat#74104
Megascript T7 kit	Ambion, Austin, TX, USA)	*Cat#AMB13345*
Experimental Models: Cell Lines		
D. melanogaster: Cell line S2: S2-DRSC	Drosophila Genomics Resource Center, Indiana University) (DGRC)	FlyBase: FBtc0000181
S2 cell line co-expressing Lgl-GFP and mCherry-Tubulin	Carvalho et al., 2015	N/A
S2 cell line co-expressing Lgl^{3A} –RFP and Lgl-GFP	This paper	N/A
S2 cell line expressing Lgl-Dendra2	This paper	N/A
Experimental Models: Organisms/Strains		
D. melanogaster: pp1-87B $^{87Bg-3}$, *pp1*α*-96A*^{2}	Bloomington Drosophila Stock Center	BDSC: #23699
		Flybase IDs: FBgn0004103
		FBal0212815

(*Continued on next page*)

Continued

REAGENT or RESOURCE	SOURCE	IDENTIFIER
D. melanogaster: lgl^{27S}	Bloomington Drosophila Stock Center	BDSC: #41561
		FlyBase ID: FBal0175616
D. melanogaster: lgl^{4}	Bloomington Drosophila Stock Center	BDSC: #36289
		FlyBase ID: FBal0009225
D. melanogaster: lglt^{s3}	Semeriva, M. (Manfruelli et al., 1996)	FlyBaseID: FBal0051412
D. melanogaster: aPKC^{k06403}	Bloomington Drosophila Stock Center	BDSC: #10622
		FlyBaseID: FBal0064438
D. melanogaster: Df(3R)Exel7357	Bloomington Drosophila Stock Center	BDSC: #7948
		FlyBase ID: FBab0038319
D. melanogaster: flw^{FP41}	Bloomington Drosophila Stock Center	BDSC: # 51338
		FlyBase ID: FBal0267524
D. melanogaster: UAS-Lgl-GFP (3rd chromosome)	Knoblich, J.A. (Betschinger et al., 2003)	N/A
D. melanogaster: UAS-Lgl-GFP (2rd chromosome – attP-VK18 insertion)	St Johnston D.	N/A
D. melanogaster: UAS-Lgl-RFP	Knoblich, J.A. (Betschinger et al., 2003)	N/A
D. melanogaster: UAS-Lgl^{3A}-GFP	Knoblich, J.A. (Betschinger et al., 2003)	N/A
D. melanogaster: UAS-AurA-GFP	J. Knoblich (Berdnik and Knoblich, 2002)	N/A
D. melanogaster: UAS-Lgl^{K327A,F331A}–GFP (2rd chromosome – attP-VK18 insertion)	This paper	N/A
D. melanogaster: UAS-AurA$^{\Delta Ab}$-GFP	Kimata, Y. (Meghini et al., 2016)	N/A
D. melanogaster: UAS-hPPP1CC	Bloomington Drosophila Stock Center	BDSC: #64394
		FlyBase ID: FBti0182016
D. melanogaster: UAS-NiPp1-HA	Bloomington Drosophila Stock Center	BDSC: #23711
		FlyBase ID: FBti0077905
D. melanogaster: UAS-*Pp1-87B RNAi*	Bloomington Drosophila Stock Center	BDSC: #32414
		FlyBase ID: FBti0132109
D. melanogaster: UAS-*sds22 RNAi*	Vienna Drosophila Resource Center	VDRC: v42051
		FlyBase ID: FBti0081237
D. melanogaster: UAS-*flw* RNAi	Bloomington Drosophila Stock Center	BDSC: #57022
		FlyBase ID:
		FBti0164842
D. melanogaster: UAS-*mts RN*Ai	Bloomington Drosophila Stock Center	BDSC: #38337
		FlyBase ID: FBti0149551
D. melanogaster: Lgl-GFP	Hong, Y. (Dong et al., 2015)	N/A
D. melanogaster: Lgl-mCherry	Hong, Y. (Dong et al., 2015)	N/A
D. melanogaster: aPKC-GFP	Schweisguth, F.(Besson et al., 2015)	N/A
Oligonucleotides		
Primers for dsRNAi (See Table S1)	This paper	N/A
RT-PCR for α-*tub* Sense (5′to 3′): CACACCACCC TGGAGCATTC	This paper	N/A
RT-PCR for α-*tub* Antisense (5′to 3′): CCAATCAG ACGGTTCAGGTTG	This paper	N/A
RT-PCR for *Pp1-87B* Sense (5′to 3′): CGATCTGTT GCGTCTGTTC	This paper	N/A
RT-PCR for *Pp1-87B* Antisense (5′to 3′): CTTGT GGATTTCGACTCGC	This paper	N/A
Cloning of Lgl^{KA,FA} Sense (5′to 3′): CTTGACTTTA CGTCTGCAGTGATTGACGCCTTTGTGAC	This paper	N/A

(*Continued on next page*)

Continued		
REAGENT or RESOURCE	SOURCE	IDENTIFIER
Cloning of Lgl^{KA,FA} Antisense (5′to 3′): AGACGT AAAGTCAAGACACACTTTGTGTCCATCGCTGG	This paper	N/A
Recombinant DNA		
pENTR-Lgl	Carvalho et al., 2015	N/A
pENTR-Lgl^{3A}	Carvalho et al., 2015	N/A
pMTW-Dendra	Gilles Hickson, University Montréal, Canada	N/A
pHWG (Drosophila Gateway Vector Collection)	Drosophila Genomics Resource Center	Gateway Collection
pHWR (Drosophila Gateway Vector Collection)	Drosophila Genomics Resource Center	Gateway Collection
pUASt.attb.WG	Brogna. S.	N/A
pMT-Lgl-Dendra2	This paper	N/A
pHW-Lgl-GFP	Carvalho et al., 2015	N/A
pHW-Lgl^{3A}-RFP	This paper	N/A
pUASt.attb.Lgl^{K327A,F331A}-GFP	This paper	N/A
pMAL-LGL$^{402-802}$	Knoblich, J.A. (Betschinger et al., 2003)	N/A
Software and Algorithms		
ImageJ/FIJI	Schindelin et al., 2012	https://fiji.sc/
Icy	Quantitative Image Analysis Unit at Institut Pasteur	http://icy.bioimageanalysis.org
EpiTools	Heller et al., 2016	N/A
MATLAB version R2016a	MathWorks	RRID: SCR_001622
GraphPad Prism	GraphPad Software	https://www.graphpad.com/scientific-software/prism/
PROMALS3D	N/A	http://prodata.swmed.edu
Jalview 2.10.5	N/A	http://www.jalview.org
Other		
Confocal microscope	Leica Microsystems, Germany	TCS SP5 II
Spinning Disk Confocal Microscope	Olympus, UK	Andor Revolution XD

CONTACT FOR REAGENT AND RESOURCE SHARING

Further information and requests for reagents may be directed to and will be fulfilled by the Lead Contact, Eurico Morais-de-Sá (eurico.sa@ibmc.up.pt).

EXPERIMENTAL MODEL AND SUBJECT DETAILS

Drosophila stocks and genetics

Drosophila melanogaster flies were cultured on standard cornmeal/agar/molasses/yeast media at 18°C or 25°C, unless otherwise noted. *tj-GAL4* and *GR1-GAL4* drivers were used to induce expression of UAS transgenes in the follicular epithelium, whereas *matα4*-GAL4-VP16 was used to induce the expression in embryos. The FLP/FRT-mediated mitotic recombination system was used to generate clones, which were induced by heat shock at 37°C. The *GAL80* repressor was used together with FLP/FRT recombination system to control the induction of *Pp1-87B RNAi* in clonal analysis (Figure 2A) and to express UAS-Lgl^{K327A,F331A}-GFP in *lgl* mutant cells (Figure 3E). Crosses were maintained at 18°C and then flies were incubated at 29°C to boost the efficiency of RNAi depletion in experiments with UAS-driven RNAi. Flies were also incubated at 29°C during 1 day for the rescue experiment in Figures 3E and 3F. Both UAS-Lgl^{K327A,F331A}-GFP (this study) and *UAS-Lgl-GFP* (unpublished, gift of Daniel St Johnston, Gurdon Institute, Cambridge, UK) were inserted into the same genomic landing site, attP-VK18. Detailed genotypes are depicted below.

Figure 1

A) *hs-FLP nls-RFP FRT19/hs-FLP tub-Gal80 FRT19; tj-GAL4/+; UAS-Lgl-GFP/+*
(clonal expression to evaluate local Lgl-GFP signal specifically in dividing cell)
B) *w*; *tj-GAL4/+*; *UAS-Lgl-GFP, HisRFP/+*
E, F) Control: *w*; *UAS-Lgl-RFP/ tj-GAL4*

UAS-AurA: *w*; *UAS-Lgl-RFP/ tj-GAL4; UAS-AurA-GFP/+*
UAS-AurAΔAb: *w*; *UAS-Lgl-RFP/ tj-GAL4*; *UAS-AurAΔAb-GFP/+*

Figure 2

A) *hs-FLP nls-RFP FRT19/hs-FLP tub-Gal80 FRT19*; *tj-GAL4/+*; *UAS-Pp1-87B RNAi/+*
B) *hs-FLP ubi-RFP-nls FRT19/flw*^{FP41} *FRT19*; ; *+/+*
hs-FLP/+;; FRT82 RFP/ FRT82 pp1α-96A^{2}
hs-FLP/+;; FRT82 RFP/ FRT82 pp1-87B^{87Bg-3} *e pp1α-96A*^{2}
C) *w; tj-GAL4/+*; *UAS-Pp1-87B RNAi/+*
w; *tj-GAL4/UAS-hPpp1cc*; *UAS-Pp1-87B RNAi/+*
D) *w; tj-GAL4 Lgl-GFP/+*; *UAS-NiPp1-HA/+*
H) *w*; *tj-GAL4/UAS-Lgl-RFP*; *UAS-Pp1-87B RNAi/UAS-Lgl*^{3A}*-GFP*

Figure 3

A) *w*; *tj-GAL4*/CyO; *UAS-Pp1-87B RNAi/+*
w; *tj-GAL4/ aPKC*^{k06403}; *UAS-Pp1-87B RNAi/+*
C) *w*; *tj-GAL4/UAS-Lgl–GFP*
w; *tj-GAL4/UAS-Lgl*^{K327A,F331A}*–GFP*
D) *w*; *tj-GAL4/UAS-Lgl–GFP*
w; *tj-GAL4/+*; *UAS-Lgl*^{3A}*-GFP/+*
w; *tj-GAL4/UAS-Lgl*^{K327A,F331A}*–GFP*
E) *hs-FLP/+*; *lgl*^{27S3} *FRT40 UAS-Lgl*^{K327A,F331A}*–GFP/ tub-GAL80 FRT40*; *GR1-GAL4/+*
(*lgl* homozygous mutant cells are the only ones expressing UAS-Lgl^{K327A,F331A}–GFP)
F) *hs-FLP/+*; *lgl*^{27S3} *FRT40/ RFP FRT40*
hs-FLP/+; *lgl*^{27S3} *FRT40 UAS-Lgl-GFP/ RFP FRT40*; *GR1-GAL4/+*
hs-FLP/+; *lgl*^{27S3} *FRT40UAS-Lgl*^{K327A,F331A}*–GFP/ RFP FRT40*; *GR1-GAL4/+*
(lgl homozygous mutant cells are marked by absence of RFP in a tissue with general expression of UAS-Lgl transgenes)

Figure 4

A,B) *w*; *tj-GAL4/+*; *UAS-Lgl-GFP, HisRFP/+*
w; *tj-GAL4/+*; *UAS-Pp1-87B RNAi/UAS-Lgl-GFP, HisRFP*
w; *tj-GAL4/UAS-sds22 RNAi*; *UAS-Lgl-GFP, HisRFP/+*
C,D) *w*; *tj-GAL4/UAS-Lgl*^{K327A,F331A}*–GFP/*;
w; *tj-GAL4/UAS-Lgl*^{K327A,F331A}*–GFP, UAS-sds22 RNAi*;
E) *aPKC-GFP*; *Lgl-mCherry*
F,G) *aPKC-GFP/+*; *lgl4* or *ts3* /+; HisRFP/+ (control)
aPKC-GFP/+; *lgl*^{ts3}*/lgl*^{4}; *HisRFP/+* (*lgl* temperature sensitive)

Figure S1

A) embryos from females: *matα4-GAL4* crossed with males: *UAS-Lgl-GFP*

Figure S2

A) *w* (control)
B) *w*; *tj-GAL4/+*; *UAS-mts RNAi/+*
C) *w*; *tj-GAL4/UAS-flw RNAi*; *+/+*
D) *w*; ; *pp1-87B*$^{87Bg-3}$ *e pp1α-96A*^{2} */ Df(3R)Exel7357*

Figure S3

aPKC-GFP/+; *CyO/+*; *UAS-Pp1-87B RNAi/+* (Control)
aPKC-GFP/+; *tj-GAL4/+*; *UAS-Pp1-87B RNAi/+* (PP1-87B RNAi)

Figure S4

B) Embryos from females: *matα4*-GAL4 crossed with males: *UAS-Lgl-GFP or UAS-Lgl*^{KAFA}*-GFP*
C) *aPKC-GFP/+*; *lgl*^{4}*/+* or *lgl*^{ts3}*/+* (Control)
aPKC-GFP/+; *lgl*^{ts3}*/lgl*^{4} (lgl temperature sensitive)

Drosophila cell culture

Drosophila Schneider 2 (S2) cells obtained from *Drosophila* Genomics Resource Center, Indiana University (DGRC) were cultured in Schneider's *Drosophila* media supplemented with 10% FBS (fetal bovine serum), at 25°C.

METHOD DETAILS

S2 cell stable lines and RNA interference

Stable S2 cell lines co-expressing Lgl-GFP and mCherry-Tubulin (Carvalho et al., 2015), co-expressing Lgl^{3A} –RFP and Lgl-GFP, or expressing Lgl-Dendra2 were generated using either Cellfectin® II reagent or Effecten Transfection Reagent, according to manufactures' instructions. Gene expression was induced at 37°C for 1 hour in cells expressing Lgl under heat-shock promoter (plasmids: pHW-Lgl-GFP and pHW-Lgl^{3A}-RFP). For double-strand RNAi production, genomic DNA was amplified using primers containing a T7 RNA polymerase-binding site flanked by gene specific sequences (see Table S1). The length of sequences amplified was: 362 bp of *aurA,* 311 bp of *aPKC*, 511 bp of *sds22* and 614 bp of *Pp1-87B.* Megascript® T7 kit was used to transcribe dsRNA from PCR amplified sequences. For RNAi treatment, S2 cells in an exponential growth phase were seeded in a serum-free Schneider media (at a concentration of 1×10^6 cells/ml) and incubated with 30 μg dsRNAi (15 μg in case of *Pp1-87B*) for 1 hour. After that, 2 mL of Schneider's growth media supplemented with 10% of FBS was added and cells analyzed after 96h or 120h.

Preparation of ovary and S2 cell protein extracts

To prepare ovary protein extracts, *Drosophila* ovaries were disrupted through sonication in Lysis Buffer (150 mM KCl, 75 mM HEPES, pH 7.5, 1.5 mM EGTA, 1.5 mM $MgCl_2$, 15% glycerol, 0.1% NP-40) containing 1x protease inhibitors cocktail (Roche) and 1x phosphatase inhibitors cocktail 3 (Sigma). For protein extracts from S2 cells, harvested cells were washed with PBS 1x supplemented with Protease Inhibitors Cocktail (Roche). Lysis buffer was then added and cells were disrupted by sonication. Samples were then centrifuged and supernatant was collected for analyses.

Immunofluorescence and F-actin staining

Drosophila ovaries were fixed using a 4% paraformaldehyde solution (in PBS), followed by washing steps with 0.05% PBT (PBS with 0.05% TWEEN® 20 (Sigma)), 1 hour-blocking with 10% BSA in 0.2% PBT, and overnight incubation at room temperature with primary antibodies diluted in 0.05% PBT (supplemented with 1% BSA). Ovaries were then washed with 0.05% PBT containing 1% BSA, incubated 2 hours with the secondary antibody and washed with 0.05% PBT before mounting in Vectashield with DAPI. The primary antibodies used are indicated in the key resources table. F-actin staining was performed by adding Phalloidin-TRITC at 1 μg/mL to the paraformaldehyde solution during the fixation.

Cloning of Lgl variants

Site-directed mutagenesis in the PP1 - docking site of Lgl was performed using primers containing the desired mutations (see Key Resources Table) and pENTR-Lgl as template (Carvalho et al., 2015). PCRs were performed using Phusion High Fidelity DNA polymerase, followed by a digestion of the template plasmid with DpnI, and transformation of competent bacteria. The Gateway Cloning System (Life Technologies) was used to generate the following plasmids: pMT-Lgl-Dendra2 - recombination of pENTR-Lgl with pMT-W-Dendra2 (gift of Gilles Hickson, University Montréal, Canada); pHW-Lgl^{3A}-RFP - recombination of pENTR-Lgl^{3A} (Carvalho et al., 2015) with pHWR; pUASt.attb.$Lgl^{K327A,F331A}$-GFP, upon recombination of pEntr-$Lgl^{K327A,F331A}$ with pUASt.attb.WG (gift of Saverio Brogna, University of Birmingham, UK). UAS-$Lgl^{K327A,F331A}$-GFP transgene was inserted into the attP-VK18 landing site on chromosome II (BDSC: #9736) via PhiC31 site-specific transgenesis (BestGene Inc).

RT-PCR

Total RNA was isolated using RNeasy Mini Kit from RNAi depleted and control S2 cells ($3x10^6$ cells) following the manufacturer's protocol. RNA samples were then used to synthetize cDNA using SuperScriptTM II Reverse Transcriptase and then PCRs for the required genes were performed using DreamTaq DNA polymerase and primers listed in the Key Resources Table.

Amplified PCR products were resolved in 1% agarose gel electrophoresis.

Protein purification

MBP-$Lgl^{402-802}$ protein was expressed in BL21 Star *E.coli* transformed with pMAL-$Lgl^{402-802}$ ((Betschinger et al., 2003), Gift of Jurgen Knoblich (IMBA, Vienna, Austria)) and purified using amylose magnetic beads according to the manufacturer's instructions (New England Biolabs).

in vitro dephosphorylation assays

For *in vitro* dephosphorylation assays using Lgl from ovary extracts (Figure 2F), Lgl-GFP was immunoprecipitated from ovary extracts using GFP-Trap_MA system according to the manufacturer's instructions. Lgl bound to the beads was then incubated with 200 ng of AurA in kinase reaction buffer (5 mM MOPS, pH 7.2, 2.5 mM β-glycerol-phosphate, 5 mM $MgCl_2$, 1 mM EGTA, 0.4 mM EDTA, 0.25 mM DTT, 100 μM ATP) during 30 min at 30°C to saturate Lgl phosphorylation status. The kinase reaction mix was removed and the phosphatase reaction mix was added, containing 2 μM MLN8237 for inhibition of the AurA kinase, PMP phosphatase buffer (New England Biolabs) containing 50mM HEPES pH 7.5, 100 mM NaCl, 2 mM DTT, 0.01% Brij 35, 1 mM $MnCl_2$ and respective amounts of recombinant human GST-PP1γ. For *in vitro* dephosphorylation assays using recombinant MBP-Lgl (Figure 2E and Figure S2E), the purified protein was first phosphorylated using the kinase assay performed as described above. Dephosphorylation

was then performed in a reaction solution containing 2 μM MLN8237, PMP phosphatase buffer containing 1 mM $MnCl_2$ (New England Biolabs), and 1U of either Protein Phosphatase 1 or Lambda PP (Figure S2E) or GST-PP1γ (Figure 2E). Dephosphorylation reactions were carried at 30°C for 30 min and stopped by addition of SDS Laemmli buffer. p-Lgl656 antibody was used to detect phosphorylation in western blot, whereas anti-GFP, anti-MBP-HRP conjugated or anti-GST were performed to control for the amount of Lgl-GFP, MBP-Lgl or PP1-GST, respectively.

Photoconversion experiments in S2 cells

For photoconversion experiments, expression of Lgl-Dendra2 in S2 cells was induced with 500 μm $CuSO_4$ for at least 12h before live imaging, and cells were plated in glass bottom microwell dishes (MaTek) coated with Poly-L-Lysine. We used Leica TCS SP5 II (Leica Microsystems) confocal microscope and a 405 nm UV laser to perform photoconversion of Lgl-Dendra2. Initial frames were taken using 488 nm and 561 nm lasers to validate photoconversion. Time-lapse stacks covering all the dividing cell were then taken using the 561 nm laser every 2 min, for at least 30 min after anaphase onset.

Multiple sequence alignments

Multiple sequence alignment of Lgl proteins from several species was performed using CLUSTAL format by PROMALS3D (http://prodata.swmed.edu) and the aligned amino acid sequences of the putative PP1-docking site motif were visualized using Jalview 2.10.5 (http://www.jalview.org). Protein sequences used were the following: *H. sapiens* LLGL1 (UniProt:Q15334); *H. sapiens* LLGL2 (UniProt:Q6P1M3); *D. rerio* LLGL1 (UniProt:E7FD67); D. rerio LLGL2 (UniProt:Q7SZE3); *S. purpuratus*predicted L2GL2 (NCBI: XP_011678406.1); *D. melanogaster* L2GL (UniProt:P08111); *N. vectensis* predicted protein (UniProt:A7RKR7); *A.queenslandica* uncharacterized protein (UniProt:A0A1X7U8H8); *S. cerevisiae* SRO7 (UniProt:Q12038).

Imaging

Fixed samples were analyzed using a Leica TCS SP5 II (Leica Microsystems) confocal microscope with HC PL APO CS 40x/NA 1.10 objective or HC PL APO CS 63x /1.30 Glycerine and a LAS 2.6 software. Live imaging was performed using a spinning disc confocal system (Andor Revolution XD) equipped with an electron multiplying charge coupled device camera (iXonEM+; Andor) and a CSU-22 unit (Yokogawa) based on an inverted microscope (IX81; Olympus) with a PLAPON 60x/NA 1.42 objective using iQ software (Andor). Z stacks were collected with serial optical sections separated by 0.5-1 μm. For live imaging of the *Drosophila* follicular epithelia, ovarioles were dissected and incubated in Schneider's media supplemented with 10% FBS and 200 μg/ml insulin (Sigma-Aldrich). Egg chambers with low expression levels of Lgl-RFP (Figures 1E and 1F) were imaged in 10S VOLTALEF® (VWR chemicals) oil for optimization of the fluorescence signal to noise. Live imaging of *Drosophila* embryos (5 to 7 hours of development; stage 10 to stage 11) was performed by immobilizing the embryos in glass bottom microwell dishes (MaTek) containing heptane glue and filled with Halocarbon oil (700) (Sigma-Aldrich). S2 cells were plated on poly-L-lysine-coated culture dishes for live imaging (MatTek). Live imaging experiments were performed at 25°C, except in experiments using the Lgl temperature sensitive mutants (lgl^{ts3}), which were filmed at 29°C.

QUANTIFICATION AND STATISTICAL ANALYSIS

Image processing and quantifications were largely performed using FIJI (Schindelin et al., 2012). All the statistical analysis and graphs were performed using GraphPad Prism 6.

Cytoplasmic decay of Lgl

Cytoplasmic decay of Lgl at mitotic exit in follicular epithelia, S2 cells and embryonic epithelia was quantified by measuring the mean pixel intensity of a manually tracked ROI in the cytoplasm (12x 12 ROI in S2 cells, 8x8 ROI in the follicular epithelia and 6x6 ROI in embryonic epithelia; 1 px = 0.13 μm) in sum-intensity Z projections. To overcome large signal fluctuation that arise from low signal intensity, we averaged 3 consecutive time points in epithelial cells (separated by 30 s) and 2 consecutive time points in S2 cells (separated by 90 s). Background subtracted mean intensity values were presented as a percentage of the anaphase value [average of the first two (in S2 cells) and three (in epithelia) frames after anaphase onset]. Since Lgl invariably reaches a steady-state with neglectable cytoplasmic intensity value in control or upon AurA overexpression/AurA RNAi, the average of the cytoplasmic intensity at the minimum plateau was subtracted in the quantifications of Figures 1 and S1 to represent cytoplasmic decay from 100% to 0%. Cytoplasmic decay has not been normalized to the minimum plateau in Figures 4, S4A, and S4B to enable the analysis of the degree of cytoplasmic accumulation induced by each genetic manipulation.

Lgl accumulation in daughter-daughter interface

To quantify the kinetics of Lgl accumulation in the daughter-daughter interface in epithelia, time-lapse images were aligned using the "StackReg" plugin and we manually tracked the interface to quantify mean intensity values since anaphase. The background subtracted mean intensity value of Lgl in the daughter-daughter interface or dividing cell equator (before cytokinesis) was normalized to the background subtracted mean intensity in the cytoplasm. The resulting anaphase value (average of the first three frames since anaphase) was set to 0% and the average intensities in the plateau of accumulation was set to 100%.

Intensity of Lgl-Dendra2 upon photoconversion

To quantify the overall intensity of Lgl-Dendra2 at mitotic exit after photoconvertion (Figure 1D) we used FIJI to perform a Z sum-projection of all optical sections covering the cell. We then used the active contour protocol of Icy (http://icy.bioimageanalysis.org) for automated cell segmentation. For each time-point, we calculated the background subtracted integrated density (cell area x mean intensity value), which is normalized to the value at anaphase onset (100%).

aPKC accumulation in the apical interface formed between daughter cells

To quantify the accumulation of aPKC in the apical daughter-daughter interface (Figure 4F), we used the image analysis toolkit EpiTools (Heller et al., 2016) to generate selective plane projections of the apical area of the follicular epithelium. The aPKC-GFP signal was then manually tracked in: 1) the equator of dividing cell/daughter-daughter interface (10 pixel width line); 2) four non dividing neighboring cell interfaces (10 pixel width line); 3) three circular ROI with 8 pixel diameter in the cytoplasm, which is used for background subtraction. We generated a custom FIJI script to measure the background subtracted mean intensities of the new daughter-daughter interface and of the non-dividing interfaces, and to normalize the signal of aPKC in the new daughter-daughter interface to the average of non-dividing ones.

Interphase cortical/cytoplasmic intensity ratio of Lgl in S2 cells

To measure the ratio of cortical to cytoplasmic mean intensity of Lgl in S2 cells during interphase (Figure 2G), we used a FIJI macro for automated segmentation of each cell contour (CC) and measured the mean intensity of the region between CC - 1 pixel and CC – 5 pixel (1 px = 0.13 μm) as the cortical intensity. Cytoplasmic intensity was measured using a circular ROI in the cytoplasm. Ratio was obtained after background subtraction.

Cell Reports, Volume *26*

Supplemental Information

PP1-Mediated Dephosphorylation of Lgl Controls Apical-basal Polarity

Sofia Moreira, Mariana Osswald, Guilherme Ventura, Margarida Gonçalves, Claudio E. Sunkel, and Eurico Morais-de-Sá

Supplemental Figures

Figure S1, related to Figure 1. Lgl cortical reloading at mitotic exit in embryonic epithelium and S2 cells

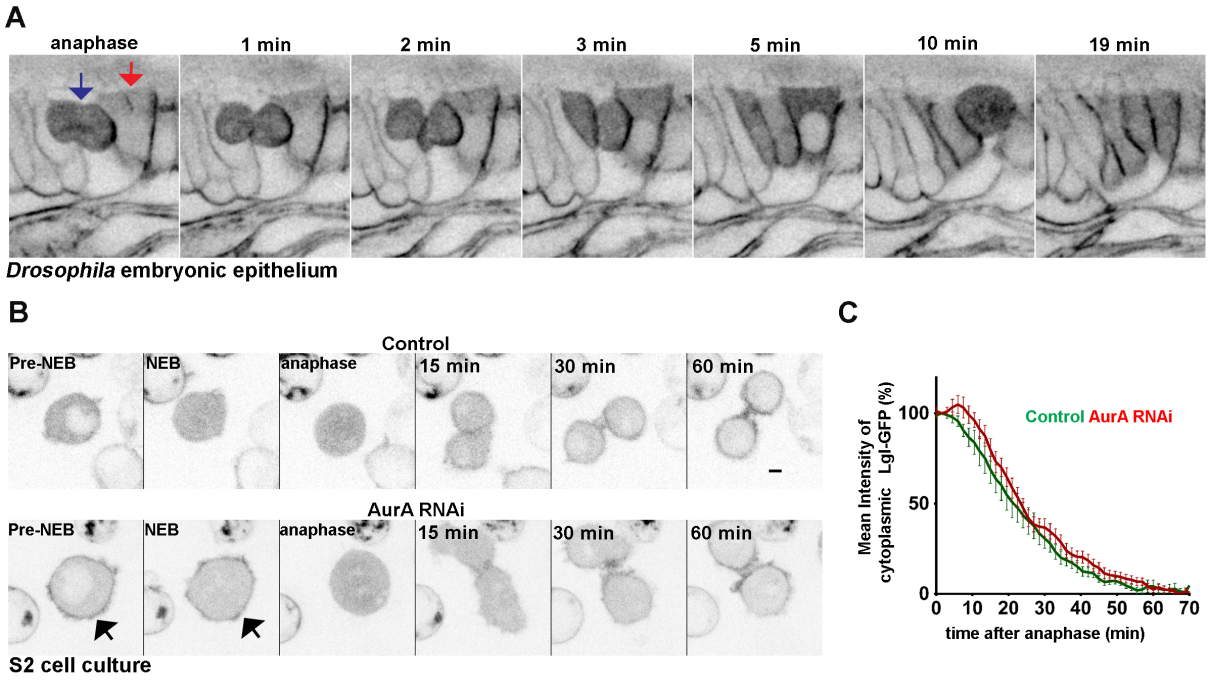

(A) Time-lapse images showing epithelial cells dividing in *Drosophila* embryos expressing Lgl-GFP (arrows). Lgl-GFP is released from the cortex to the cytoplasm prior to nuclear envelope breakdown (NEB) (cell indicated by the red arrow), and then relocates to the preexistent cortex and to the daughter-daughter interface formed during cytokinesis. Time is relative to the anaphase of the cell indicated by the blue arrow. Scale bar, 5 µm

(B,C) Downregulation of AurA activity is not the timer controlling Lgl cortical reloading at mitotic exit. (**B)** Time-lapse images of dividing *Drosophila* S2 cells expressing Lgl-GFP and depleted of AurA by RNAi. Lgl-GFP is retained in the cortex at nuclear envelope breakdown (NEB) in AurA-depleted cells (arrows) as anticipated from AurA role on Lgl cortical release at mitotic entry, but cortical reloading at mitotic exit is not affected by AurA RNAi. Scale bar = 5 µm **(C)** Lgl-GFP cytoplasmic decay in AurA-depleted cells (n=17) and control cells (n=22) was used as a proxy for Lgl cortical reloading. Plot shows mean intensity value of Lgl-GFP in the cytoplasm ± SEM (the mean of the post-mitotic minimum intensity was subtracted and all intensity values were normalized to the average of the first two frames after anaphase onset (%)). Lgl cortical retention at mitotic entry (NEB) was monitored to ensure that only cells efficiently depleted of AurA were quantified.

Figure S2, related to Figure 2. Pp1-87B antagonizes aPKC/AurA phosphorylation to control Lgl localization

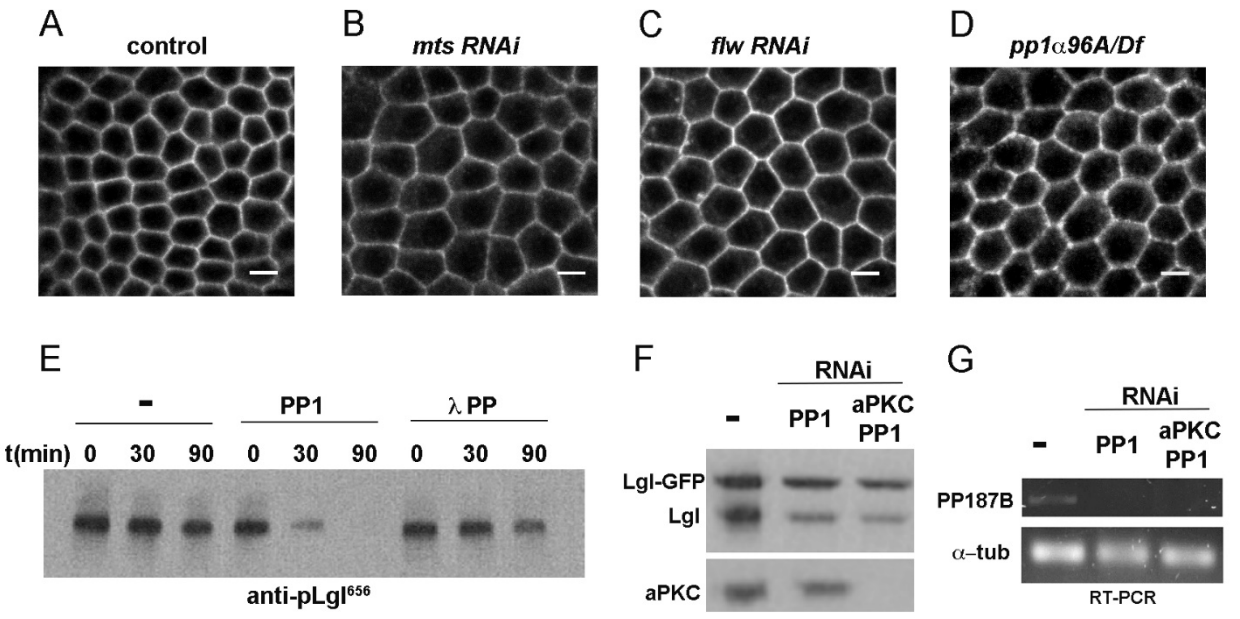

(A-D) Immunofluorescence images of endogenous Lgl show that, contrarily to *Pp1-87B* depletion or loss of function (Figure 2), RNAi-mediated depletion of the catalytic subunit of PP2A (*mts* RNAi*,* 81% egg chambers show normal cortical localization, n=40) or flapwing (*flw* RNAi*,* 89% egg chambers with normal cortical localization, n=64) does not have a major impact on Lgl cortical localization in the follicular epithelium. Complete loss of *Pp1α-96A* function in transheterozygous follicle cells harboring a chromosome deletion removing the *pp1α-96A* loci (*Df(3R)Exel7357*) over the null *pp1α-96A*^{2} allele also shows normal cortical localization of Lgl (97% egg chambers with normal cortical localization, n=70).

(E) *In vitro* phosphatase assay comparing dephosphorylation efficiency of recombinant MBP-Lgl previously phosphorylated by AurA using 1U (accordingly to their activity to a non-specific substrate (p-nitrophenyl phosphate)) of PP1 or λ phosphatase. Phosphorylation was monitored by western blot using an antibody specific for phosphorylated Ser656. (**F)** Western blot showing efficient depletion of aPKC in S2 cells (related to Figure 2G). (**G)** RT-PCR confirms efficient depletion of PP1 in cells treated with PP1-87B dsRNA and with both PP1-87B and aPKC dsRNA (related to Figure 2G). Scale bars, 5 µm

Figure S3, related to Figure 3. PP1-87B is required to preserve the monolayered architecture of the follicular epithelium

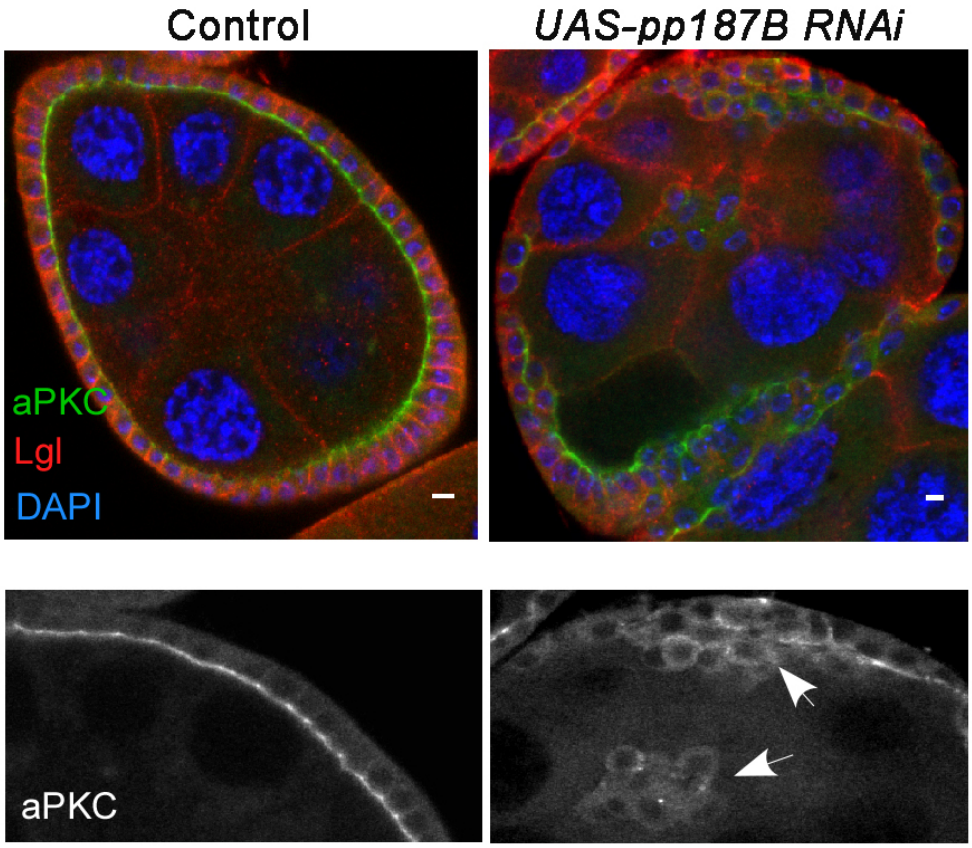

Egg chambers expressing aPKC-GFP (green) at endogenous levels and depleted of PP1-87B by RNAi driven in the follicular epithelium were stained for Lgl (red) and DAPI (blue). PP1-87B RNAi induces loss of epithelial polarity in the follicular epithelium, multilayering and invasion of epithelial cells in-between the germline (white arrows). Scale bars, 5 µm

Figure S4, related to Figure 4.

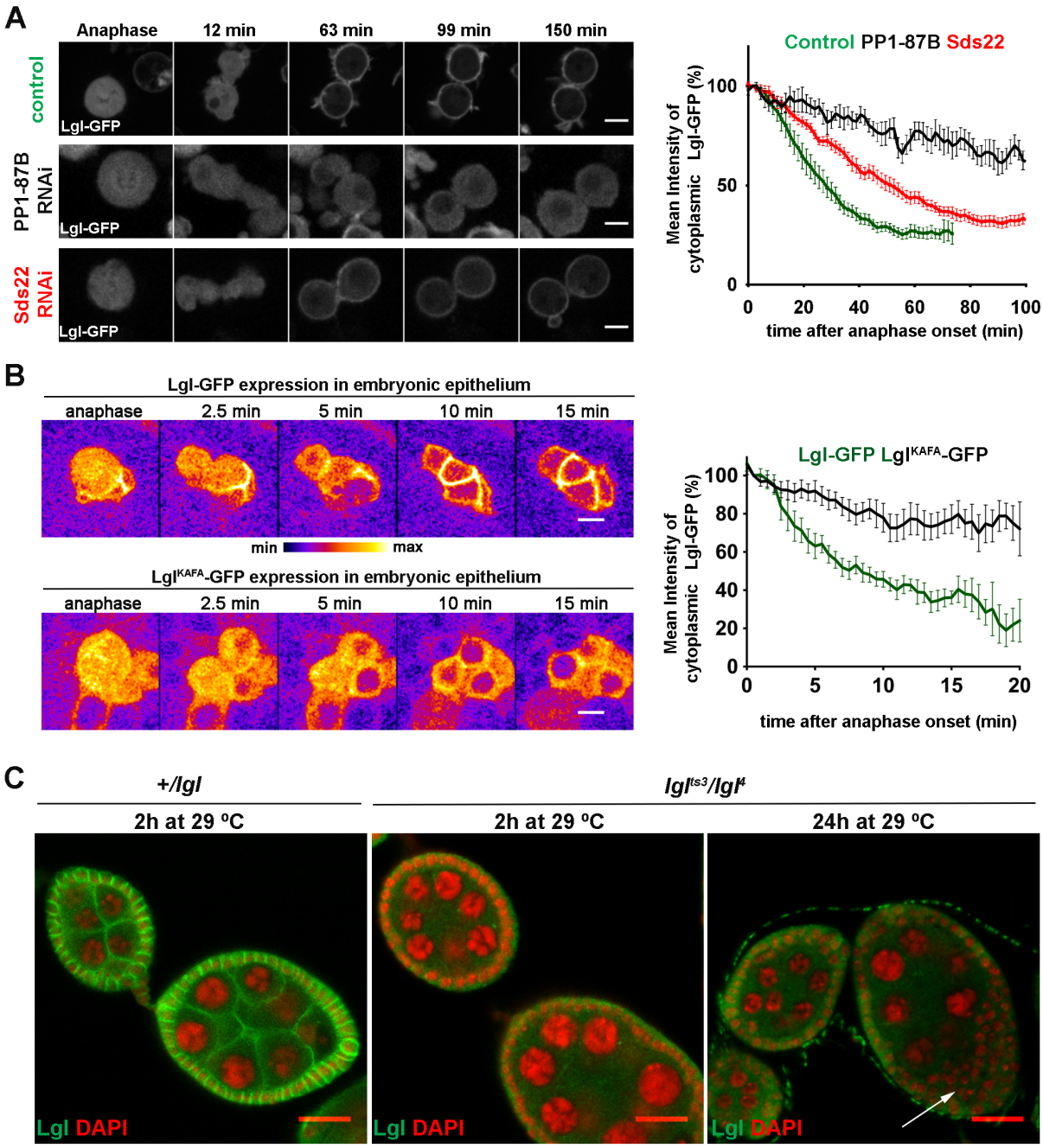

A) The PP1/Sds22 complex is necessary for efficient reloading of Lgl at mitotic exit in S2 cells. Time-lapse images show that depletion of either PP1-87B or the regulatory subunit Sds22 delays Lgl-GFP reloading to the cortex at mitotic exit. Plot shows mean intensity value of Lgl-GFP in the cytoplasm ± SEM (background subtracted mean intensity values were normalized to the average cytoplasmic levels for the first two frames since anaphase onset (%) of control (n=23), PP1-87B RNAi (n=10) and Sds22 RNAi (n=19). Despite the slower kinetics of cytoplasmic decay in cells depleted of Sds22, Lgl ultimately reaches almost normal cytoplasmic levels during interphase. Scale bars, 5 µm

B) Lgl^{KA,FA}-GFP strongly accumulates in the cytoplasm in embryonic epithelial cells. Plot represents Lgl-GFP (n=11) and Lgl^{KAFA}-GFP (n=9) mean cytoplasmic intensity in cells of the outer epithelial layer of stage 10 to stage 11 embryos. Error bars indicate SEM. Scale bar, 5 μm

C) A temperature sensitive allele of Lgl induces full cytoplasmic localization at restrictive temperature. Lgl immunofluorescence (green) in egg chambers of *lgl^{ts3}/lgl^{4}* and sibling flies carrying a wild-type copy of Lgl (lgl$^{ts3 \text{ or } 4}$/+) and raised at the indicated temperatures. Lgl^{ts3} is completely reallocated to the cytoplasm after 2h at 29ºC without disruption of the monolayered organization of the follicular epithelium, whereas strong multilayering of the epithelial tissue arises after longer incubation at restrictive temperature (arrow). DAPI (red) labels the cell nucleus. Scale bars, 20 μm

Table S1. List of primers used in this study for RNAi, related to STAR Methods

Purpose	Sense/Antisense (5'<>3')	
dsRNA synthesis	*aurA*	TAATACGACTCACTATAGGGACTACTTGCCACCCGAAATG
		TAATACGACTCACTATAGGGAATTAAATTACGCGGGGAGCA
	aPKC	TAATACGACTCACTATAGGGACCCGTTCCTGGTCGGATTG
		TAATACGACTCACTATAGGGACCGCAGAATGTGGAGGTGGT
	sds22	TAATACGACTCACTATAGGGAGAACTTGTCCAGCCTGAA
		TAATACGACTCACTATAGGGTTCTTGGCCAAGTCGAGG
	Pp1-87B	TAATACGACTCACTATAGGGTCGGAAATTAAAGATTTCGAGG
		TAATACGACTCACTATAGGGAAGATCTTCTCGTCGACAATGG